

Electronic Supplementary Information

## **Light-guided Electrodeposition of Non-Noble Catalyst Patterns for Photoelectrochemical Hydrogen Evolution**

Sung Yul Lim,<sup>a</sup> Yang-Rae Kim,<sup>a</sup> Kyungyeon Ha,<sup>b,c</sup> Jong-Kwon Lee,<sup>c</sup> Jae Gyeong Lee,<sup>a</sup>

Woohyuk Jang,<sup>a</sup> Jin-Young Lee,<sup>a</sup> Je Hyun Bae,<sup>a</sup> and Taek Dong Chung<sup>\*,a,d</sup>

<sup>a</sup>Department of Chemistry, Seoul National University, Seoul 08826, Korea

<sup>b</sup>Department of Mechanical and Aerospace Engineering, Seoul National University, Seoul 08826, Korea

<sup>c</sup>Global Frontier Center for Multiscale Energy Systems, Seoul National University, Seoul 08826, Korea

<sup>d</sup>Advanced Institutes of Convergence Technology (AICT), Suwon-Si, Gyeonggi-do 16229, Korea

*\*Correspondence and requests for materials should be addressed to T.D.C.*

*(email: tdchung@snu.ac.kr)*

# Contents

## List of figures

1. Optical images of electrodeposited dot-shaped Pt pattern taken before and after the washing process.
2. Current-time curve at -0.4 V (vs. Ag/AgCl) for light-guided electrodeposition of Pt.
3. Effects of dynamic light pattern generated by light-guided electrodeposition of Pt.
4. Linear sweep voltammograms for hydrogen evolution reaction (HER) at bare a-Si photocathode under light and dark conditions.
5. Energy-dispersive X-ray spectroscopy (EDS) spectra of Pt, Au, and Au/Pt nanoparticles generated by electrodeposition.
6. Scanning electron microscope (SEM) images of light-induced electrodeposited Pt line pattern obtained by scanning substrate.
7. Local photocurrent in deaerated pH 4.5 buffer due to Ni-Mo pattern.
8. Capacitance-voltage curves recorded for a SiO<sub>x</sub>/a-Si photocathode.
9. Optimization of amount of Ni-Mo catalyst for each spacing values on a-Si photocathode.
10. Histograms of the photocurrent at 0 V vs. reversible hydrogen electrode (RHE) with various amounts of Ni-Mo loading at each of the different spacings.
11. Cross-sectional SEM images of Ni-Mo films with different optimal amounts for different spacings.
12. Variation in the total spectral reflectance of Ni-Mo pattern/SiO<sub>x</sub>/a-Si with spacing.
13. Linear sweep voltammograms for various spacing of Ni-Mo dots under constant pattern diameter, 130 μm.
14. Calculation of applied-bias photon-to-current efficiency (ABPE).
15. HER performance for various *D/S* values at Ni-Mo pattern/SiO<sub>x</sub>/a-Si photocathodes from LSV.
16. Calculation of incident photon-to-current conversion efficiency (IPCE).

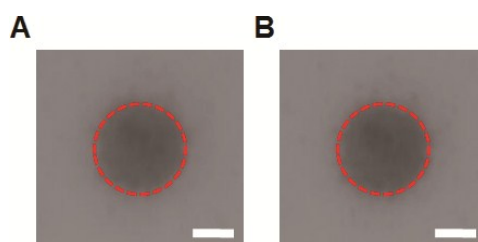


**Fig. S1** Optical images of electrodeposited dot-shaped Pt pattern captured (A) before and (B) after washing process. Dotted lines in red represent the illuminated area with laser (Scale bar: 5  $\mu\text{m}$ ).

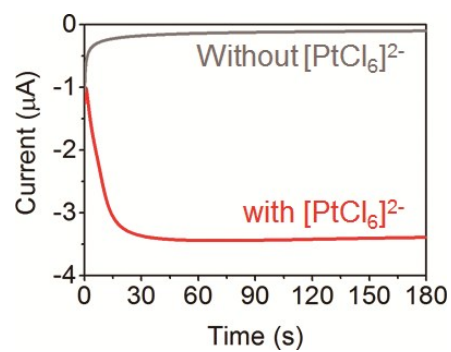


**Fig. S2** Current-time curve recorded at -0.4 V (vs. Ag/AgCl) for 180 s. Red and gray lines represent the *i-t* curve in the presence and absence of Pt precursors in electrolyte solutions, respectively.

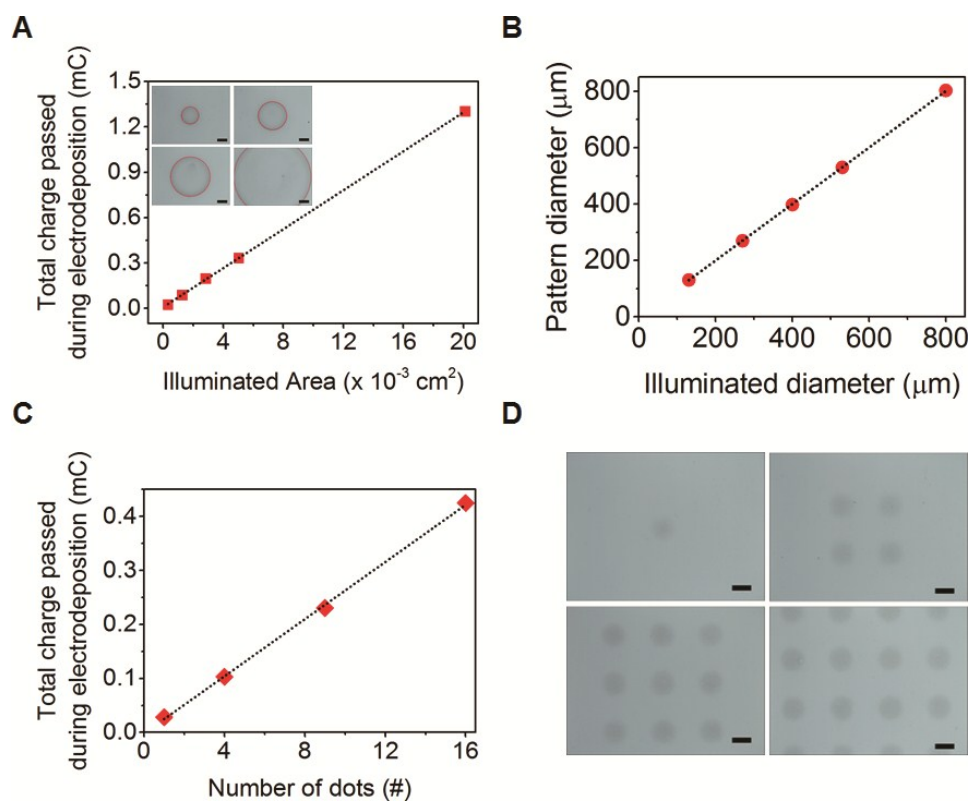


**Fig. S3** Effects of dynamic light pattern generated by 625 nm LED and DMD display on light-guided electrodeposition of Pt at -0.4 V (vs. Ag/AgCl) for 180 s. (A) Total charge passed during Pt electrodeposition under light with various diameters (Scale bar in inset images: 100  $\mu\text{m}$ ). The total charge was calculated by subtracting the integrated area of  $i-t$  curve in the absence of Pt precursors from in the presence of them. (B) Linear correlation between illuminated area and the size of pattern electrodeposited by light on a-Si (slope:  $1.00 \pm 0.02$  and intercept:  $0.044 \pm 0.026$  with an  $R^2 = 0.999$ ). The diameters of the electrodeposited patterns were measured by the ImageJ program. (C) Linear increase of total charge passed during electrodeposition of Pt with the number of light spots represented by the circle. (D) Optical images of Pt spots electrodeposited by light (Scale bar: 400  $\mu\text{m}$ ).

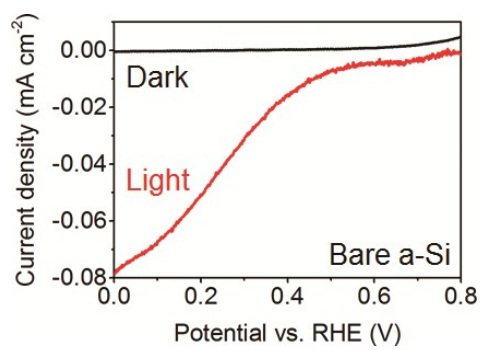


**Fig. S4** Linear sweep voltammograms for HER at bare a-Si photocathode under light and dark conditions.

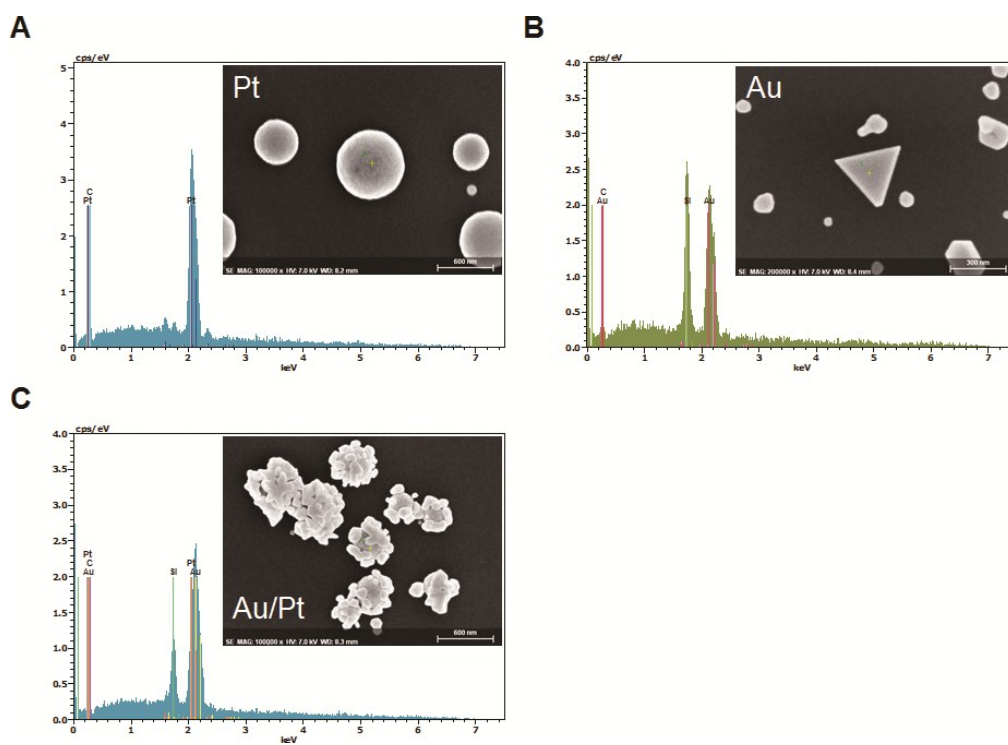


**Fig. S5** EDS spectra of Pt, Au, and Au/Pt nanoparticles generated by electrodeposition. The Pt nanoparticles were deposited prior to Au electrodeposition and the Au particles electroplated on the illuminated area. Au/Pt represents the Au nanoparticles electrodeposited on the pre-patterned Pt nanoparticles.

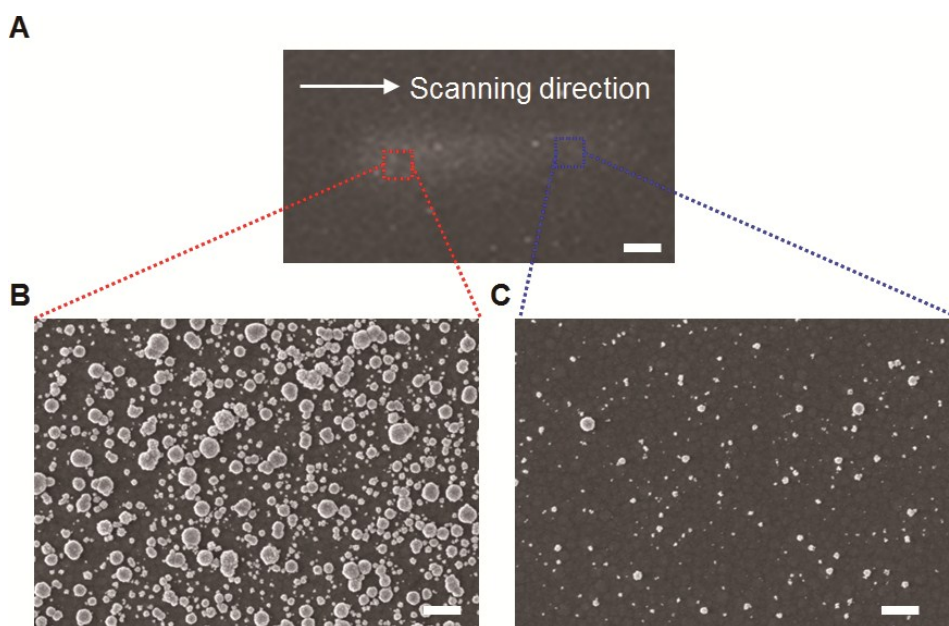


**Fig. S6** SEM images of light-induced electrodeposited Pt line pattern obtained by scanning substrate under bias at  $-0.4$  V (vs. Ag/AgCl). Substrates were moved at a rate of  $1 \mu\text{m s}^{-1}$ . **B** and **C** show the area where the scanning starts and ends, respectively (scale bar in **A**:  $5 \mu\text{m}$ , **B** and **C**:  $200 \text{nm}$ ).

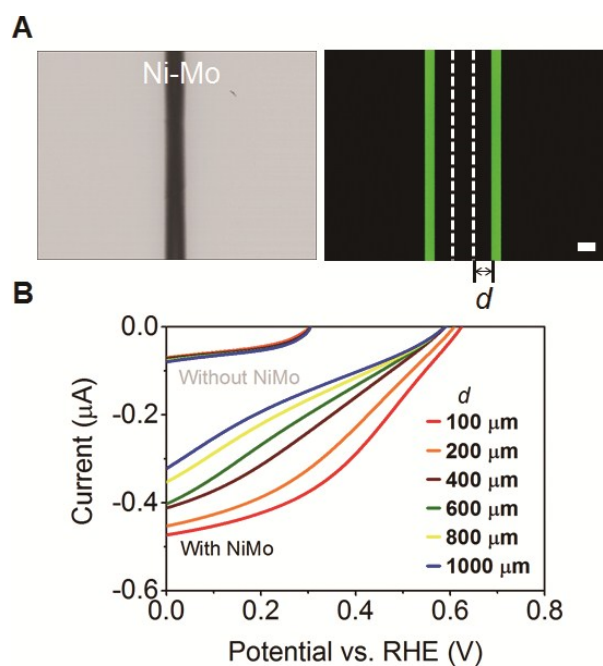


**Fig. S7** Local photocurrent in deaerated pH 4.5 buffer due to Ni-Mo pattern. (A) Left: optical image of a line of electrodeposited Ni-Mo. Right: scheme of local photocurrent measurement under 530 nm LED illumination generated by DMD (scale bar: 100  $\mu\text{m}$ ). (B) LSVs to probe local PEC activity as a function of illumination distance from the Ni-Mo, which acts as an electron collector. LSVs under the same conditions without the Ni-Mo pattern are presented for comparison.

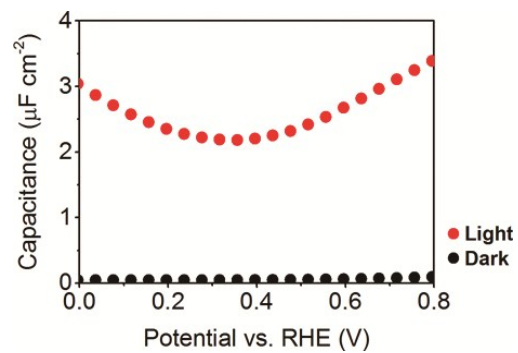


**Fig. S8** Capacitance-voltage curves recorded for a  $\text{SiO}_x/\text{a-Si}$  photocathode under simulated AM 1.5 illumination and dark conditions measured at 100 Hz AC frequency.

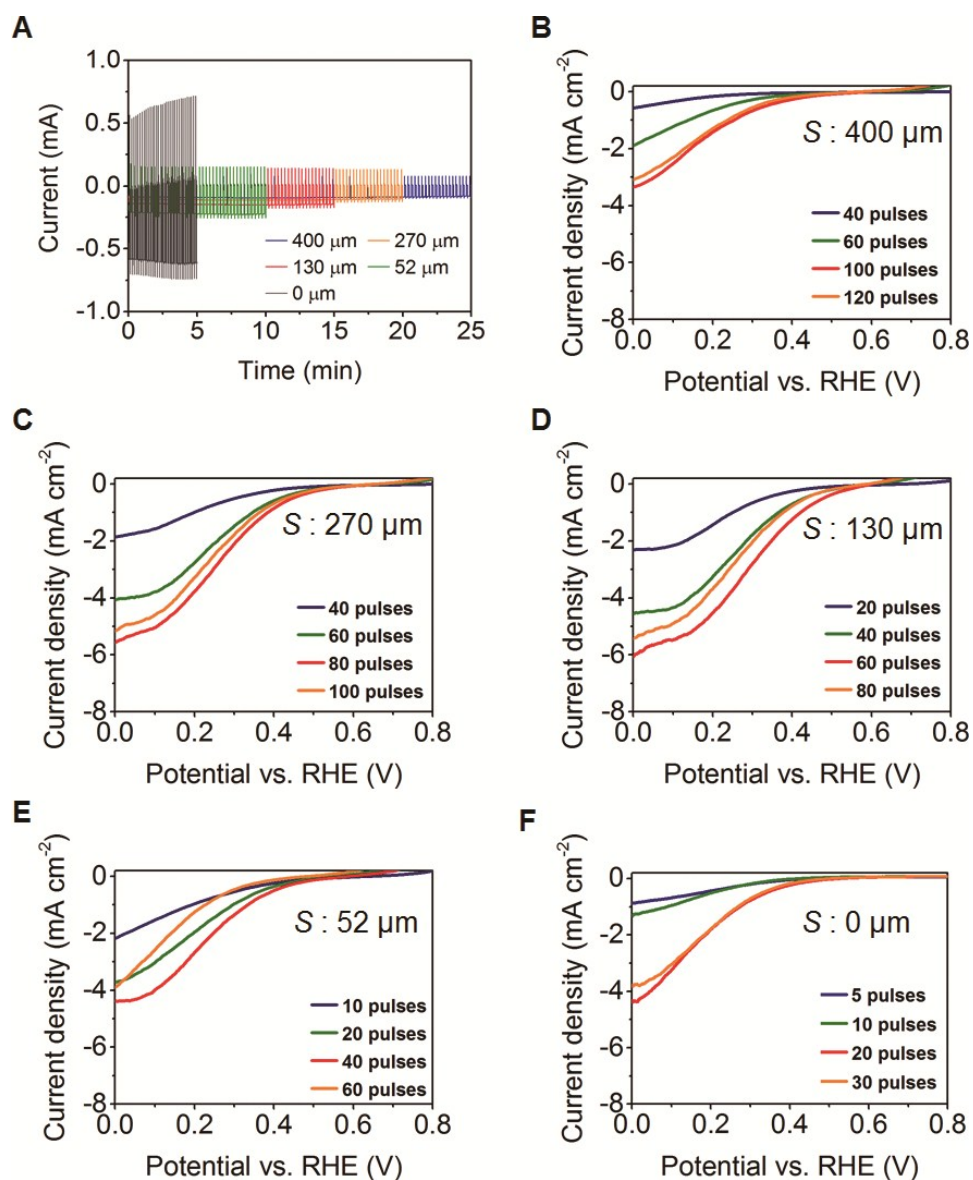


**Fig. S9** Optimization of amount of Ni-Mo catalyst for each spacing value on a-Si photocathode. (A) Current-time (*i-t*) curves for optimized light-guided electrodeposition of Ni-Mo with various spacing. The results of LSV for different amounts of Ni-Mo loaded, which were controlled by the number of reduction pulses. The spacing was varied at (B) 400, (C) 270, (D) 130, (E) 52 μm, and (F) 0 μm under simulated AM 1.5 illumination. The diameter of all Ni-Mo dots was constant, 400 μm.

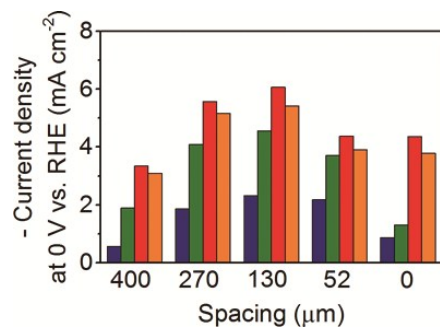


**Fig. S10** Histograms of the photocurrent at 0 V (vs. RHE) with various amounts of Ni-Mo loading at each of the different spacings (Histogram colors correspond to the number of the potential pulses presented in panel **B-E** of **Fig. S8**).

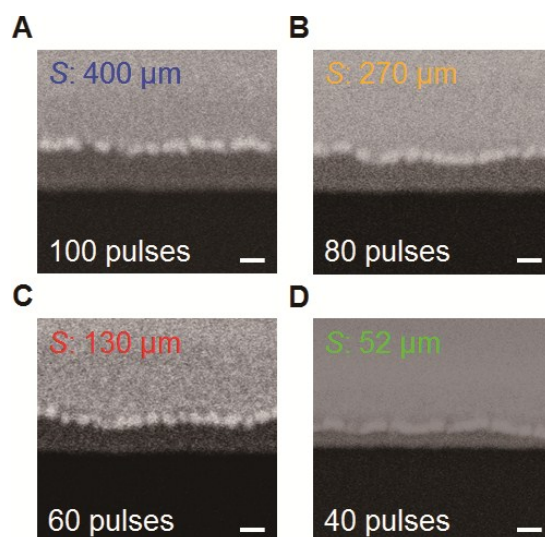


**Fig. S11** Cross-sectional SEM images of Ni-Mo films with different optimal amounts for different spacings. The optimized thicknesses were roughly (A) 150 nm, (B) 100 nm, (C) 80 nm, and (D) 50 nm (scale bar is 100 nm).

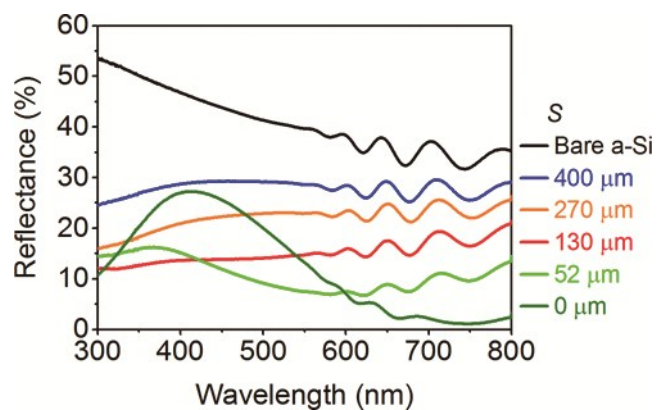


**Fig. S12** Variation in the total spectral reflectance of Ni-Mo pattern/SiO<sub>x</sub>/a-Si with spacing, in which the diameter of Ni-Mo catalyst was constant, 400 μm. Here 0 μm refers to the a-Si substrate whose surface was fully covered with Ni-Mo catalyst.

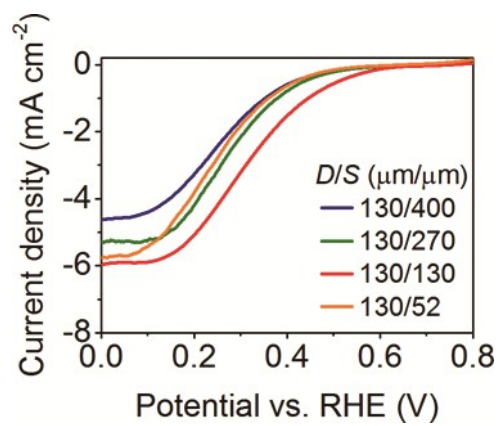


**Fig. S13** Linear sweep voltammograms for various spacing of Ni-Mo dots under constant pattern diameter, 130  $\mu\text{m}$ .

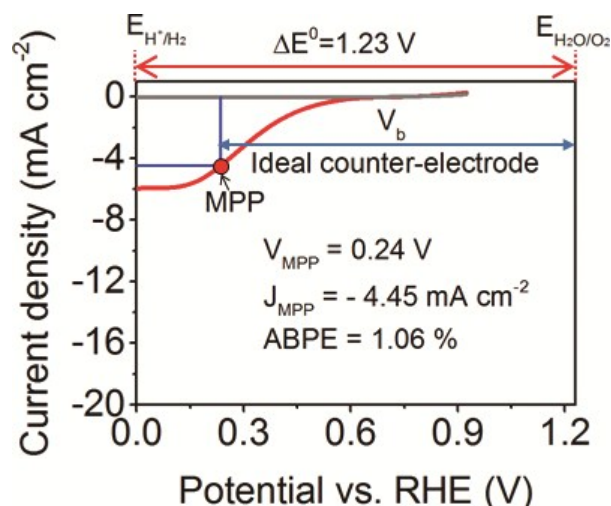


**Fig. S14** Calculation of ABPE. For evaluating ABPE, linear sweep voltammograms were recorded in deaerated pH 4.5 buffer solutions at  $100 \text{ mV s}^{-1}$  under AM 1.5 illumination. Typical equations for calculating ABPE are given by the following<sup>1,2</sup>:

$$ABPE = \left[ \frac{|J (\text{mA cm}^{-2})| \times (1.23 - |V_b|)(V)}{I (\text{mW cm}^{-2})} \right] \times 100 \% \quad (1)$$

where  $J$  is the photocurrent density,  $V_b$  is the potential versus ideal counter electrode, and  $I$  is the incident illumination intensity ( $100 \text{ mW cm}^{-2}$  in this work). We present the ideal ABPE here, which assumes an ideal counter electrode for maximum power point (MPP). The equation for ABPE (ideal) is given by<sup>1,2</sup>:

$$ABPE (\text{Ideal counter electrode}) = |J_{MPP} \times V_{MPP}| \quad (2)$$

where  $J_{MPP}$  and  $V_{MPP}$  are the photocurrent density and potential at the MPP, respectively. The best ABPE, 1.06%, (at  $D/S = 130/130 \text{ }\mu\text{m}$ ) is presented here as an example.

		$D/S,$ $\mu\text{m}/\mu\text{m}$	Coverage factor, $\pi D^2/4(S+D)^2$	$J$ (at $V=0$ vs. RHE), $\text{mA cm}^{-2}$	$V_{\text{OC}}$ (at $J = -0.1 \text{ mA cm}^{-2}$ ), $V$ vs. RHE	$V_{\text{MPP}},$ $V$ vs. RHE	$J_{\text{MPP}},$ $\text{mA cm}^{-2}$	ABPE, %
$\begin{array}{c} \uparrow S \text{ variation} \\ \downarrow D \text{ variation} \end{array}$	$D : 400 \mu\text{m}$	400/400	0.20	-3.34	0.49	0.17	-1.72	0.29
		400/270	0.28	-5.56	0.57	0.21	-3.57	0.76
		400/130	0.45	-5.98	0.57	0.22	-4.08	0.94
		400/52	0.61	-4.38	0.52	0.17	-2.88	0.54
	$D : 130 \mu\text{m}$	130/400	0.047	-4.62	0.55	0.20	-3.20	0.64
		130/270	0.083	-5.29	0.56	0.20	-4.17	0.84
		130/130	0.20	-5.98	0.62	0.24	-4.45	1.06
		130/52	0.40	-5.76	0.53	0.19	-4.06	0.77
	$D \text{ variation}$	1200/130	0.64	-4.73	0.53	0.19	-2.71	0.52
		800/130	0.58	-5.52	0.55	0.20	-3.33	0.65
		400/130	0.45	-5.98	0.57	0.22	-4.08	0.94
		270/130	0.36	-5.99	0.61	0.23	-4.22	0.95
130/130		0.20	-6.00	0.62	0.24	-4.45	1.06	

**Fig. S15** HER performance for various  $D/S$  values at Ni-Mo pattern/ $\text{SiO}_x/\text{a-Si}$  photocathodes from LSV. MPP denotes maximum power point.

**Fig. S16** Calculation of IPCE. For calculating IPCE, steady-state photocurrent density was measured at 0 V (vs. RHE) under monochromatic illumination generated by a Xe arc lamp and monochromator. The IPCE in this study was determined referring to the formula shown below<sup>1, 2</sup>:

$$IPCE = \frac{1239.8 (V \text{ nm}) \times |J (mA \text{ cm}^{-2})|}{P_{mono} (mW \text{ cm}^{-2}) \times \lambda (nm)} \quad (3)$$

where  $P_{mono}$  is the monochromated illumination power density and  $\lambda$  denotes the wavelength.

## References

1. D. V. Esposito, I. Levin, T. P. Moffat and A. A. Talin, *Nat. Mater.*, 2013, **12**, 562-568.
2. L. Ji, M. D. McDaniel, S. Wang, A. B. Posadas, X. Li, H. Huang, J. C. Lee, A. A. Demkov, A. J. Bard, J. G. Ekerdt and E. T. Yu, *Nat. Nanotechnol.*, 2015, **10**, 84-90.